# Supporting Information

## Zinc-tetracarboxylate framework material with nano-cages and one-dimensional channels for excellently selective and effective adsorption of methyl blue dye

Qipeng Li,[a,b] Jinjie Qian,*[c] Lin Du,*[a] and Qihua Zhao*[a]

[a]*Key Laboratory of Medicinal Chemistry for Natural Resource Education Ministry, School of Chemical Science and Technology, Pharmacy, Yunnan University, Kunming, 650091, P.R. China.*

[b]*Science and Technology Department, College of Chemistry and Chemical Engineering, Zhaotong University, Zhaotong, 657000, P. R. China.*

[c]*College of Chemistry and Materials Engineering, Wenzhou University, Wenzhou, 325035, P. R. China.*

**Supercritical Carbon Dioxide (SCD) Drying**[S1]

First of all, as-obtained single crystals of **FJI-11** are evacuated with supercritical $CO_2$ in a Tousimis Samdri-PVT-3D instrument. Prior to the activation process, the as-synthesized DMA/1,4-dioxane solvated **FJI-11** samples are soaked in pure acetonitrile solvent (MeCN), and refreshing the soaking solution every day for 5 days, in order to fully exchange the occluded solvent for MeCN. After the completed MeCN-exchange process, the MeCN-solvated samples are immediately placed inside the pressure vessel and the MeCN is exchanged with liquid $CO_2$ by opening the "FILL" button over a period of 3 hours, in which the $CO_2$ (liquid) is vented from 1100 psi to 1000 psi by very slowly unlocking the "BLEED" button for 5 minutes each 30 minutes. And then close the "BLEED" button and the chamber pressure return to 1100 psi, please notice the chamber temperature by adjusting the upper-left "COOL" button as well. After 3 hours of repeatedly venting and soaking with $CO_2$ (liquid) the chamber is sealed and the temperature is raised to 40 °C.

This would bring the chamber pressure to around 1300 psi above the critical point of $CO_2$. The chamber is then held above the critical point for another 3 hours at which point the chamber is slowly vented overnight (12 hours). Then the dried samples are quickly transported into an adsorption tube in the glove box. The PXRD patterns of supercritical $CO_2$ exchanged **FJI-11** samples confirm that it retains the highly crystalline and then are tested for nitrogen adsorption soon.

## Adsorption capability of FJI-11 towards organic dye[S2]

In order to investigate the dye adsorption and separation behaviors in **FJI-11**, the methyl orange (MO), methylene blue (MB), rhodamine 6G (R6G) and rhodamine B (RB) with different sizes and configurations were chosen for the adsorption experiments (Figure S7). The prepared crystalline samples (10 mg) of **FJI-11** were immersed in the dye-containing acetonitrile solution (10 mg/L), at constant temperature oscillations for a certain time, the concentrations of the organic dyes before and after adsorption were menstruated by UV/Vis spectrophotometer.

Sequence standard MB acetonitrile solution with the concentration of 0.1, 2, 4, 6, 8, 10, 12 and 14 mg/L were prepared and their absorbance were measured under the $\lambda_{max}$ = 664 nm, then draw the standard curve as $A$ = 0.19029 $C_e$ + 0.04425, $R^2$ = 0.99908.

According to the formula (1), the adsorption capacity $q_e$ of **FJI-11** are calculated.

$$q_e = (c_0 - c_e)V/m \quad (1)$$

Where $c_0$ is the initial concentration of organic dye (mg/L), $c_e$ is the concentration of organic dye solution after adsorption (mg/L), $V$ is the volume of organic dye solution (L), $m$ is the amount of **FJI-11** used as adsorbents (mg) and $q_e$ is the adsorption capacity of **FJI-11** (mg/g).

10 mg **FJI-11** was added into the 10 ml methylene blue solution with the concentration of 10 mg/L for adsorption experiment under the 25 °C. After oscillating for different time, the absorbance of the methylene blue residual solution was determined by the UV/Vis spectrophotometer

According to the second order kinetic equation (2), the kinetic relationship in the adsorption of methylene blue by the **FJI-11** was calculated.

$$t/q_t = 1/k_2q_e^2 + t/q_e \quad (2)$$

Where $q_t$ is the adsorption capacity of **FJI-11** at $t$ time, $q_e$ is the adsorption capacity of **FJI-11** when the adsorption process reaches equilibrium, $k_2$ is the kinetic rate constant and $t$ is the adsorption time.

10 mg **FJI-11** was added into the 10 ml methylene blue solutions with different initial concentrations (1.0, 2.5, 7.5, 10, 12.5 and 15 mg/L) for adsorption experiments under 25 °C. After oscillating for 30 min, the absorbance of methylene blue residual solution was determined by the UV/Vis spectrophotometer.

According to the Freundlich equation (3), the thermodynamic relationship in the adsorption of methylene blue by the **FJI-11** was calculated.

$$\ln q_e = \ln K_F + 1/n \ln c_e \quad (3)$$

Where $q_{max}$ is the maximum adsorption capacity (mg/g), $q_e$ is the equilibrium adsorption capacity (mg/g), $K_F$ is the adsorption constant of Freundlich equation, $n$ is the constant related to temperature and $c_e$ is the concentration of methylene blue solution in adsorption equilibrium (mg/L).

Table S1 Selected bond distances and angles of **FJI-11**

| **FJI-11** | | | |
|---|---|---|---|
| Zn1—Zn1$^{i}$ | 2.9560 (14) | Zn1—O2 | 2.030 (4) |
| Zn1—O1$^{ii}$ | 2.028 (4) | Zn1—O2$^{iii}$ | 2.030 (4) |
| Zn1—O1$^{i}$ | 2.028 (4) | Zn1—O3 | 1.961 (7) |
| O1$^{i}$—Zn1—Zn1$^{i}$ | 80.43 (13) | O1$^{ii}$—Zn1—O2$^{iii}$ | 159.0 (2) |
| O1$^{ii}$—Zn1—Zn1$^{i}$ | 80.43 (13) | O2$^{iii}$—Zn1—Zn1$^{i}$ | 78.60 (14) |
| O1$^{ii}$—Zn1—O1$^{i}$ | 89.0 (3) | O2—Zn1—Zn1$^{i}$ | 78.59 (14) |
| O1$^{i}$—Zn1—O2$^{iii}$ | 88.4 (2) | O2—Zn1—O2$^{iii}$ | 86.5 (3) |
| O1$^{ii}$—Zn1—O2 | 88.4 (2) | O3—Zn1—Zn1$^{i}$ | 178.2 (3) |
| O1$^{i}$—Zn1—O2 | 159.0 (2) | O3—Zn1—O1$^{i}$ | 100.8 (3) |
| C5—O1—Zn1$^{i}$ | 126.9 (4) | O3—Zn1—O1$^{ii}$ | 100.8 (2) |
| C5—O2—Zn1 | 129.5 (4) | O3—Zn1—O2 | 100.1 (2) |
| Zn1—O3—H3A | 113.3 | O3—Zn1—O2$^{iii}$ | 100.1 (2) |
| Zn1—O3—H3B | 114.1 | | |

Symmetry codes: (i) −x+1, −y+2, −z; (ii) x−y+1, −y+2, −z; (iii) −x+y, y, z; (iv) −x+1/3, −y+5/3, −z−1/3; (v) −y+1, −x+1, z; (vi) −x+y, −x+1, z; (vii) −y+1, x−y+1, z.

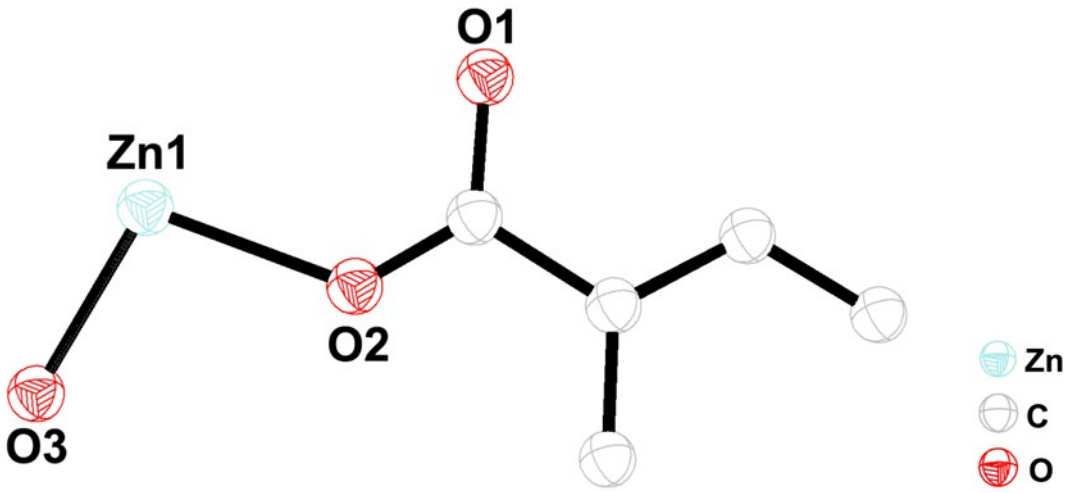


**Figure S1** The asymmetric unit of **FJI-11**. Hydrogen atoms are omitted for charity and thermal ellipsoids are also given at the 45% probability level.

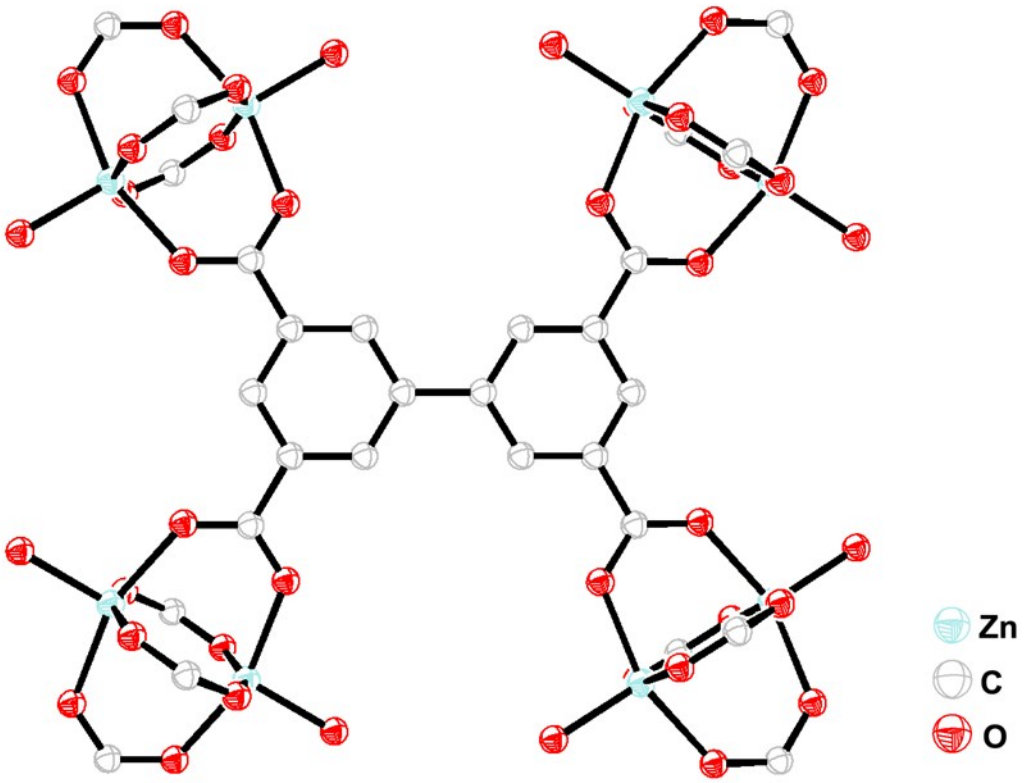


**Figure S2** View of the coordination environments of $abtc^{4-}$ ligand, Zn(II) ions and $Zn_2(COO)_4$ paddlewheel SBUs in **FJI-11**.

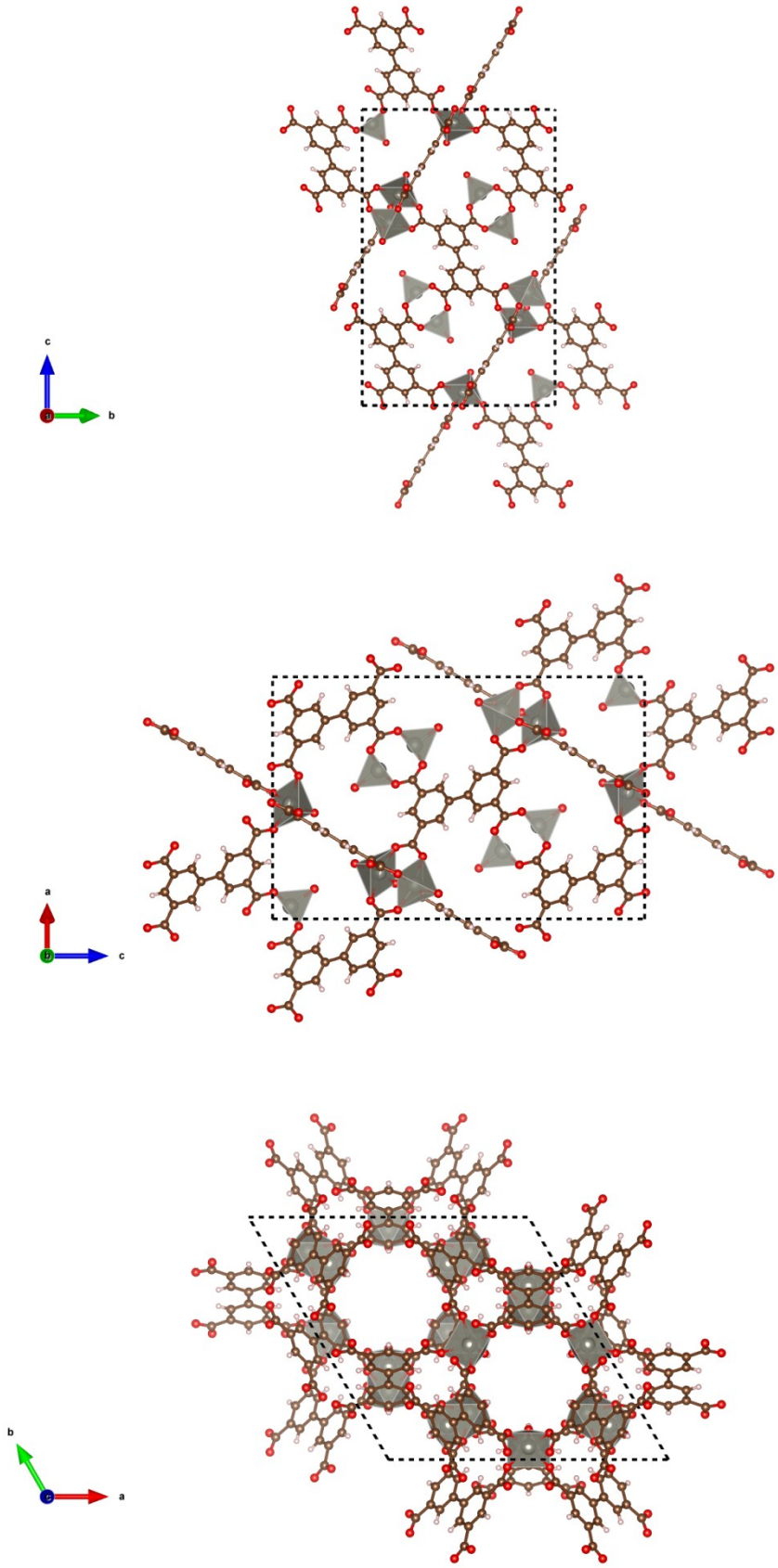


**Figure S3** The 3D cage-stacking framework in **FJI-11** under the different directions.

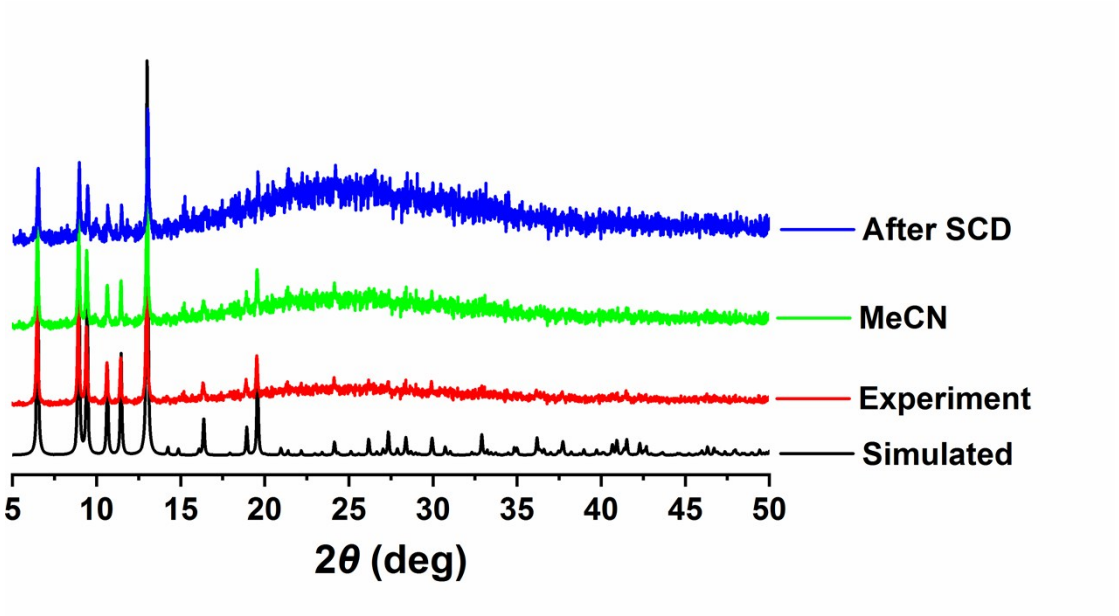


**Figure S4** The PXRD patterns of **FJI-11**.

The phase purity and stability of **FJI-11** was confirmed by powder X-ray diffraction (XRD) analysis, all the diffraction peaks of the experimental patterns are corresponding well with their simulated XRD patterns, indicating the phase purity of the as-synthesized samples (Figure S4). In addition, the diffraction peaks in MeCN and after supercritical carbon dioxide (SCD) are also corresponding well with their simulated XRD patterns, exposing the stability of **FJI-11**.

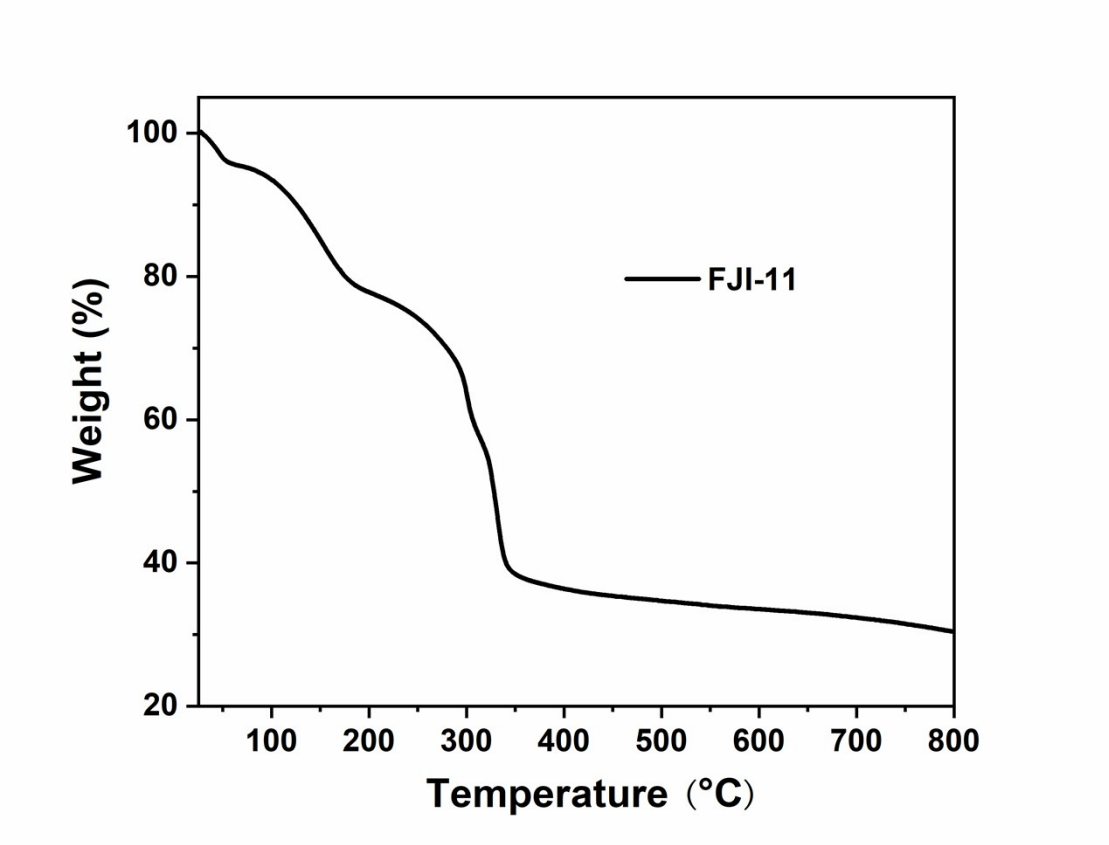


**Figure S5 The** TGA curve in **FJI-11**.

Thermogravimetric analysis (TGA) measurements are conducted in the temperature range of 30-800 °C under a flow of nitrogen with the heating rate of 10 °C $min^{-1}$. The TGA curve of **FJI-11** has a weight loss of 42.15% from 25 to 310 °C due to the loss of two coordinated water molecules and five guest DMA molecules (calcd 41.34%), and then the framework begins to decompose upon further heating (Figure S5).

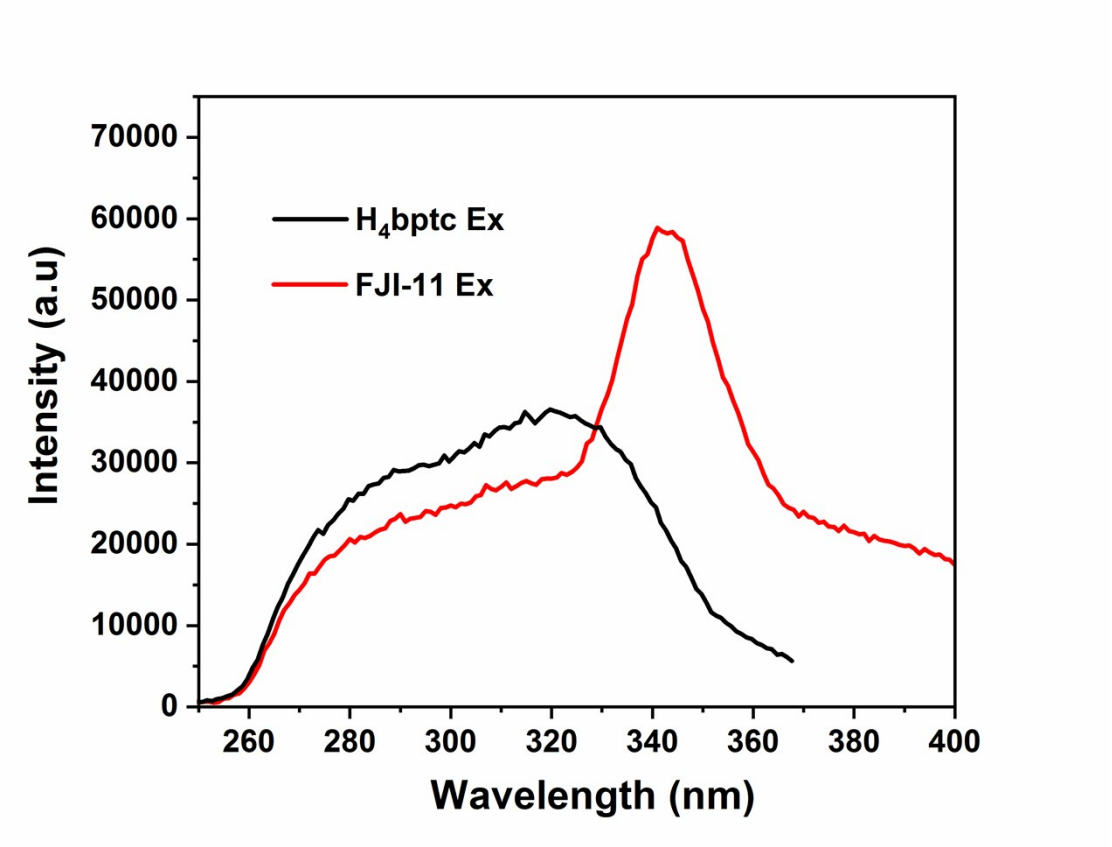


**Figure S6** Solid excitation spectra of the free $H_4$BPTC ligand and **FJI-11**.

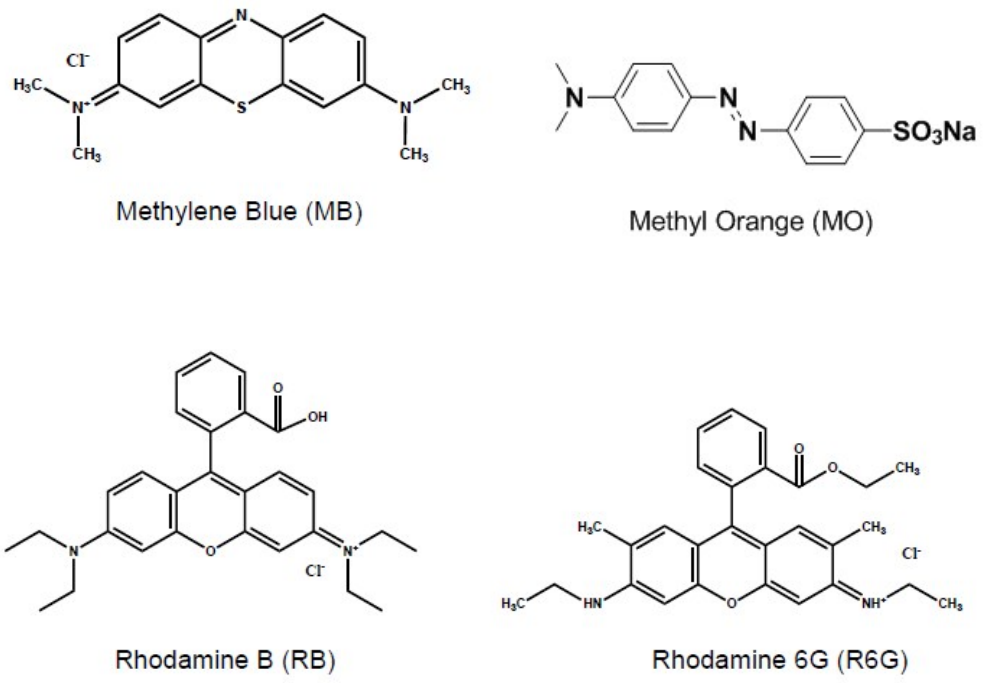


**Figure S7** Chemical structures of the organic dyes used in this work.

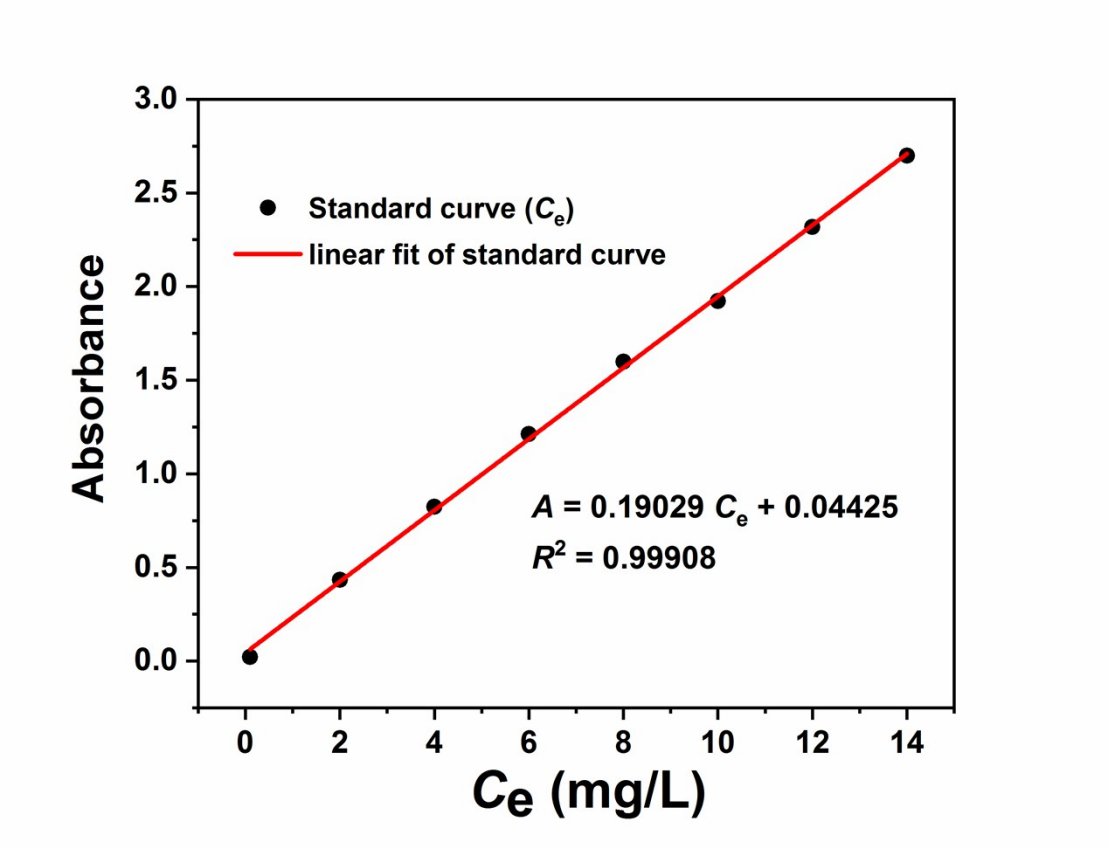


**Figure S8** The standard curve of (methyl blue) MB.

Table S2 Selective adsorption of organic dye and their adsorption mechanism in the different MOFs materials

| MOFs | Selective Adsorption of Organic Dye | Adsorption Mechanism | Ref. |
|---|---|---|---|
| InOF-9 | Methyl Blue (MB) | Cation Exchange | S1b |
| $Cd_4(H_4L)_2(phen)_2(H_2O)_4$ | Congo red (CR) | Hydrogen Bonding | S3 |
| FJI-H21 | Methylene Blue (MB), Ethyl Violet (EV) and Cation Red (GTL) | Cation Exchange | S4 |
| FJI-H-U1 | Ethyl Violet (EV), Janus Green B(JGB), and Rhodamine B (RB) | Cation Exchange | S5 |
| FJI-Y6 | Acid orange 7 (AO7) | Anion Exchange | S6 |
| MIL-68 (In) | Congo red (CR) | π–π Interaction | S7 |
| Ce(III)-doped UiO-66 | Congo red (CR) | π–π Interaction | S8 |
| Cu-BTC | Methyl Blue (MB) | Hydrogen Bonding | S9 |
| $[Cu(bipy)X]_n$ | Acid orange 7 (AO7) | Hydrophobic Adsorption and π–π Interaction | S10 |
| 1-3 | Rhodamine 6G (R6G) and Brilliant blue R (BBR) | Pore-size-dependent Molecule-selective Capture | S11 |
| Zn-1 | Rhodamine B (RB) and Crystal Violet (CV) | Size Effect of the Host and Guest Molecules | S12 |
| MIL-53 (Al) | Methylene Blue (MB) and Malachite Green (MG) | Hydrogen Bonding | S13 |
| Acid-promoted UiO-66 | Methyl Blue (MB) and Rhodamine B (RB) | Electrostatic Attraction | S14 |
| Ln(III)-MOFs | Methylene Blue (MB) | Ion-Exchange | S15 |
| $\{[Co(TBC)Cl_{0.5}(CH_3OH)]\cdot 0.5Cl\}_n$ | Methylene Blue (MB) | Ion-Exchange | S16 |
| Compounds 1 and 3 | Methylene Blue (MB) | Ion-Exchange | S17 |
| **FJI-11** | **Methyl Blue (MB)** | **Hydrogen Bonding** | **This work** |

## Reference


S1 (a) A. P. Nelson, O. K. Farha, K. L. Mulfort, J. T. Hupp, *J. Am. Chem. Soc.,* **2009**, 131, 458-460; (b) P. P. Yu, Q. P. Li, Y. Hu, N. N. Liu, L. J. Zhang, K. Z. Su. J. J. Qian, S. M. Huang and M. C. Hong, *Chem. Commun.,* **2016**, 52, 7978.

S2 (a) J. H. Qiu, Y. Feng, X. F. Zhang, M. M. Jia and J. F. Yao, *J. Coll. and Inter. Sci.,* **2017**, 499, 151; (b) Q. Chen, Q. Q. He, M. M. Lv, Y. L. Xu, H. B. Yang, X. T. Liu, F. Y. Wei, *Applied Surface Science.,* **2015**, 327, 77.

S3 J. Ai, H. R. Tian, X. Min, Z. C. Wang and Z. M. Sun, *Dalton Trans.,* **2020**, DOI: 10.1039/c9dt01545k.

S4 P. Huang, C. Chen, M. Y. Wu, F. L. Jiang and M. C. Hong, *Dalton Trans.,* **2019**, 48, 5527-5533.

S5 F. L. Hu, Z. Y. Di, P. Lin, P. Huang, M. Y. Wu, F. L. Jiang and M. C. Hong, *Cryst. Growth Des.,* **2018**, 18, 576-580.

S6 M. Zhou, Z. F. Ju and D. Q. Yuan, *Chem. Commun.,* **2018**, 54, 2998-3001.

S7 L. N. Jin, X. Y. Qian, J. G. Wang, H. Aslan and M. Dong, J. *Colloid Interface Sci.,* **2015**, 453, 270-275.

S8 J. M. Yang, R. J. Ying, C. X. Han, Q. T. Hu, H. M. Xu, J. H. Li, Q. Wang and W. Zhang, *Dalton Trans.,* **2018**, 47, 3913-3920.

S9 S. Lin, Z. Song, G. Che, A. Ren, P. Li, C. Liu and J. Zhang, *Microporous Mesoporous Mater.,* **2014**, 193, 27-34.

S10 L. Xiao, Y. Xiong, Z. Wen and S. Tian, *RSC Adv.,* **2015**, 5, 61593-61600.

S11 P. Z. Li, X. J. Wang, S. Tan, C. Ang, H. Chen, J. Liu, R. Zou and Y. Zhao, *Angew. Chem. Int. Ed.,* **2015**, 54, 12748-12752.

S12 Y. Y. Cui, J. Zhang, L. L. Ren, A. L. Cheng and E. Q. Gao, *Polyhedron.,* **2019**, 161, 71-77.

S13 C. Li, Z. h. Xiong, J. M. Zhang and C. S. Wu, *J. Chem. Eng. Data.,* **2015**, 60, 3414-3422.

S14 J. H. Qiu, Y. Feng, X. F. Zhang, M. M. Jia and J. F. Yao, *Journal of Colloid and Interface Science.,* **2017**, 499, 151-158.

S15 M. L. Gao, W. J. Wang, L. Liu, Z. B. Han, N. Wei, X. M. Cao and D. Q. Yuan, *Inorg. Chem.,* **2017**, 56, 511-517.

S16 M. Z. Wu, J. Y. Shi, P. Y. Chen, L. Tian and J. Chen, *Inorg. Chem.,* **2019**, 58, 3130-3136

S17 X. J. Gao, G. H. Sun, F. Y. Ge and H. G. Zheng, *Inorg. Chem.,* **2019**, 58, 8396-8407.